European Polymer Journal 176 (2022) 111390

Contents lists available at ScienceDirect

European Polymer Journal

journal homepage: www.elsevier.com/locate/europolj

The Role of Multilayer Electrospun Poly(Vinyl Alcohol)/Gelatin nanofibers loaded with Fluconazole and Cinnamaldehyde in the Potential Treatment of Fungal Keratitis

Elif Ilhan [a,b], Sumeyye Cesur [a], Rabia Betul Sulutas [a,c], Esra Pilavci [a,c], Basak Dalbayrak [d], Elif Kaya [e], Elif Damla Arisan [d], Gulgun Bosgelmez Tinaz [e], Mustafa Sengor [a,c], Ewa Kijeńska-Gawrońska [f,g], Faik Nuzhet Oktar [a,b], Oguzhan Gunduz [a,c,*]

[a] Center for Nanotechnology & Biomaterials Application and Research (NBUAM), Marmara University, Turkey
[b] Department of Bioengineering, Faculty of Engineering, Marmara University, Turkey
[c] Department of Metallurgical and Materials Engineering, Faculty of Technology, Marmara University, Turkey
[d] Department of Biotechnology, Institute of Biotechnology, Gebze Technical University, Gebze, Kocaeli, Turkey
[e] Department of Basic Pharmaceutical Sciences, Faculty of Pharmacy, Marmara University, Istanbul 34668, Turkey
[f] Centre for Advanced Materials and Technologies CEZAMAT, Warsaw University of Technology, Poland
[g] Faculty of Materials Science and Engineering, Warsaw University of Technology, Poland

ARTICLE INFO

Keywords:
Fungal keratitis
Nanofiber
Fluconazole
Cinnamaldehyde
Cornea tissue engineering

ABSTRACT

Fungal keratitis is a severe corneal infection that causes irreversible damage to the cornea, for which conventional drug treatments may be insufficient. With the new generation of drug delivery systems, it is desired to ensure the ocular usability of drugs. In this study, two-layer polyvinyl alcohol and gelatin (PVA/GEL) nanofibers with high drug loading capacity were produced by the electrospinning method. Cinnamaldehyde (CA), an FDA-approved volatile molecule found in cinnamon essential oil, and fluconazole (FLU), an antifungal drug, were incorporated into PVA/GEL nanofibers to inhibit the growth and biofilm formation of *Candida albicans*, one of the pathogens that cause fungal keratitis. The morphology, chemical structures, and thermal transitions of the produced pure (PVA/GEL), FLU loaded (PVA/GEL/FLU), CA loaded (PVA/GEL/CA), and combined FLU and CA loaded (PVA/GEL/COM) nanofibers were analysed by scanning electron microscopy (SEM), Fourier-transform infrared spectroscopy (FT-IR) and differential scanning calorimetry (DSC), respectively. The mechanical analysis, swelling and degradation behaviour, and drug release kinetics of the nanofibers were investigated. PVA/GEL/FLU, PVA/GEL/CA and PVA/GEL/FLU/COM nanofibers were evaluated for their antifungal and antibiofilm activity against *Candida albicans*. Results showed that PVA/GEL/FLU and PVA/GEL/COM nanofibers have significant antifungal activity and inhibited biofilm formation by 37% and 49%, respectively. Furthermore, it was determined by MTT analysis using a human embryonic kidney (HEK) that the nanofibers were not cytotoxic. In the treatment of fungal keratitis, double-layer PVA/GEL/COM nanofiber with CA in the first layer and FLU in the second layer can create a new treatment approach as an alternative drug delivery system.

1. Introduction

The cornea is the main refractive and protective layer of the eye. Inflammation of the cornea due to physical, chemical and infectious causes is known as keratitis. Due to its diverse presentation, overlapping symptoms and rapid progression, microbial keratitis has long been difficult for physicians. Keratitis is mainly associated with bacterial and viral microorganisms invading the corneal stroma. Although bacterial keratitis is the most common disease, there has been a steady increase in fungal keratitis due to multiple overlapping factors, which cause significant ocular morbidity [1]. Fungi are one of the most challenging species to diagnose and treat among the organisms that cause keratitis. Moreover, fungal keratitis has been proven to be more virulent and destructive than keratitis caused by bacterias [2]. According to the retrospective analysis, it has been shown that fungal keratitis is more likely to pierce the cornea than bacterial keratitis and causes severe

* Corresponding author.
E-mail address: ucemogu@ucl.ac.uk (O. Gunduz).

https://doi.org/10.1016/j.eurpolymj.2022.111390
Received 30 May 2022; Received in revised form 27 June 2022; Accepted 30 June 2022
Available online 9 July 2022

irreversible damage [3,4]. Fungal keratitis is mainly caused by filamentous fungi (Fusarium spp and Aspergillus spp) and yeast (Candida spp) [5]. Fungi's primary virulence characteristics that protect it against treatment agents are surface hydrophobicity, good adhesion, hydrolytic enzyme production, germ tube formation, and biofilm formation capacity [6]. Biofilms are communities of surface adherent cells surrounded by an extracellular matrix and are crucial to the development of infection. Many clinically relevant fungi produce biofilms, including *Candida* spp and *Aspergillus* spp [7]. Biofilms increase resistance to antifungal agents and protect pathogens from the host immune system, making them extremely difficult to eradicate [8].

The treatment efficacy of fungal keratitis is restricted compared to another infectious keratitis due to individual differences in response to conventional therapy [9]. Fluconazole (FLU), a synthetic bistriazole, is considered one of the safest antifungal drugs, has good intraocular penetration, and is an agent used in deeply lesioned fungal keratitis. FLU has been proven to be effective, especially in treating fungal keratitis in patients who do not respond to natamycin or miconazole [10]. But the fungistatic nature and the development of resistance have limited the use of FLU. With the increasing incidence of resistance in human pathogens and toxicity problems, treating fungal infections with conventional antifungal agents is becoming progressively more difficult gradually becoming. Therefore, there is a need for novel, effective, and less toxic antifungal drugs. Several studies have shown promising antifungal activity of some plant essential oils against fungi such as *Candida albicans* [11]. Cinnamaldehyde (CA) is a significant component of *Cinnamomum zeylanicum (Lauraceae) extract* and is widely used as a flavouring substance. It has also been reported to have antioxidant, anti-inflammatory, and anticancer properties. Furthermore, it exhibits antimicrobial and antifungal activities [12]. However, the volatile nature of CA limits its applications in the biopharmaceutical field. Thus its encapsulation within micro and nano scales vehicles is one of the methods which can provide it with physical stability. In particular, in recent years, electrospun nanofibers have been used as drug delivery systems due to their porous structure, increased surface area, and extraordinary drug loading capacity [13,14].

Electrospinning is a tissue engineering technique that uses various polymers to produce nanofibers consisting of an extensive network of interconnected fibers and pores that allow drug loading. The high porosity of electrospun nanofibers allows the efficient exchange of nutrients and metabolic wastes between patches and their surroundings [15,16]. Electrospun nanofibers produced from natural and synthetic polymers have been found to be promising, especially in wound healing treatments as drug delivery systems [17]. PVA is a synthetic polymer that is frequently utilised in many different tissue engineering applications (including corneal disease treatment) due to its biocompatible structure, good oxygen permeability, and drug loading efficiency [16,18]. Gelatin (GEL), a natural polymer that mimics the fibrous structure of the corneal stroma, provides tissue regeneration and, cause of its hydrophilic nature, allows body fluids to penetrate particles and improves the release of bioactive molecules mediated by diffusion [19,20]. Jain et al. study showed that ciprofloxacin-loaded-PVA/GEL blend solution allowed for the production of nanofibers with more controlled antibiotic release compared to conventional eye drops used in the treatment of corneal ulcers and other corneal infectious diseases [21].

In this study, two-layer PVA/GEL nanofibers loaded with different biological agents, which accelerate wound closure by suppressing the disadvantages of traditional methods in the treatment of fungal keratitis, were produced by the electrospinning method. The first layer is designed in order to inhibit the biofilm formation caused by *Candida albicans* with the nanofiber loaded with CA. Then, the second layer, loaded with FLU, provides the additional anti-fungal effect that accelerates the treatment. The originality of this study lays in the design of the multilayer electrospun nanofibers, which are loaded with both biofilm inhibitor agent and an antifungal drug. This kind of construct can be utilised in the treatment of fungal keratitis and to produce patches that accelerate wound healing and allow controlled release of the bio-active agents.

2. Material and methods

2.1. Materials

Poly (vinyl alcohol) with Mw of about 89,000–98,000 (99+% hydrolysed), Gelatin from bovine skin (powder, gel strength ~225 g bloom, Type B), Tween 80 (viscous liquid), Glutaraldehyde solution (GA, 50 wt%. MW = 100.12 g/mol) and phosphate buffer saline (PBS, pH = 7.4) were purchased from Sigma-Aldrich (St. Louis, MO, USA). *Candida albicans* (ATCC 90023) used in this study were grown on Sabouraud dextrose agar (SDA) and Methylene Blue Dye Medium at 37 °C for antimicrobial activity test. Yeast Extract Peptone Dextrose (YEPD) medium and RPMI 1640 medium with glutamine were used for the biofilm experiment. FLU (MW = 306.27 g/mol) and CA were purchased from Sigma-Aldrich, Darmstadt, Germany.

2.2. Preparation of electrospinning solutions

Solutions containing different drugs were prepared as shown in Table 1. PVA powder was dissolved in 20 ml of distilled water at 90 °C and mixed for about 1 h with magnetic stirring (Wise Stir®, MSH-20 A, Germany) to obtain a 13 % wt. solution. Later, 3 wt% of Tween 80 was added dropwise to the PVA solution, and the solution was stirred for another 15 min. Following that, 0.5 wt% GEL from bovine skin was added to the solution, and the solution was stirred for 15 min at 60 °C. Two different types of drugs, namely FLU, and CA to varying concentrations of 0.2%, and 2.6 wt%, respectively, were added separately to the 13 wt% PVA solutions. These mixtures of separate solutions were stirred for 30 min.

2.3. Electrospinning of nanofibers

A laboratory-scale electrospinning device (NS24, Inovenso Co., Türkiye) was used for the electrospinning process. Before starting the electrospinning process, the prepared solution was transferred into the syringe. To keep the flow rate of the solution under control, the syringe was in the syringe pump. Thin tubes were attached between the syringe and the needle to transfer the solution. A high-voltage power supply was attached to the the tip of the needle and the collector to provide the electrical potential difference. Waxed paper was wrapped around the cylindrical collector positioned 12 cm above the floor for the collection of nanofibers. With the solution sent from the syringe pump, production was carried out at a flow rate of 0.5 ml/h and under 25 kV voltage for 7 h. The wax paper on which the resulting nanofibers were collected was removed from the device and weighed. The drugs were not mixed within one solution when producing the combined fibres. Drugs were spun in individual layers in combined fibres for a more effective release. The solution containing 0.2 wt% of FLU in the first layer was electrospun for 3 h and 30 min. After that, the solution containing 2.6 wt% of CA was electrospun for another 3 h and 30 min at the same flow rate and voltage. The PVA/GEL/COM fibers production was completed in 7 h by loading the different drugs within separate layers of the nanofibrous mesh. The schematic representation was demonstrated in Fig. 1.

2.4. Crosslinking process

All of the produced electrospun nanofibers were crosslinked by exposition to glutaraldehyde vapours. The nanofibers were placed over the glutaraldehyde solution and incubated in an oven at 60° for 3 h.

2.5. Scanning electron microscopy (SEM)

To characterise the morphology of the non-drug and drug-loaded

Table 1
Contents of the solutions used to produce all types of electrospun nanofibers.

Electrospun nanofiber		PVA content (wt%)	GEL content (wt%)	Tween 80 (wt%)	Drug Amount (wt%)
Non-drug	PVA/GEL	13	0.5	3	–
Flucanozole	PVA/GEL/FLU	13	0.5	3	0.2
Cinnamaldehit	PVA/GEL/CA	13	0.5	3	2.6
Fluconazole Cinnemaldehyde	PVA/GEL/COM	13	0.5	3	0.2 + 2.6

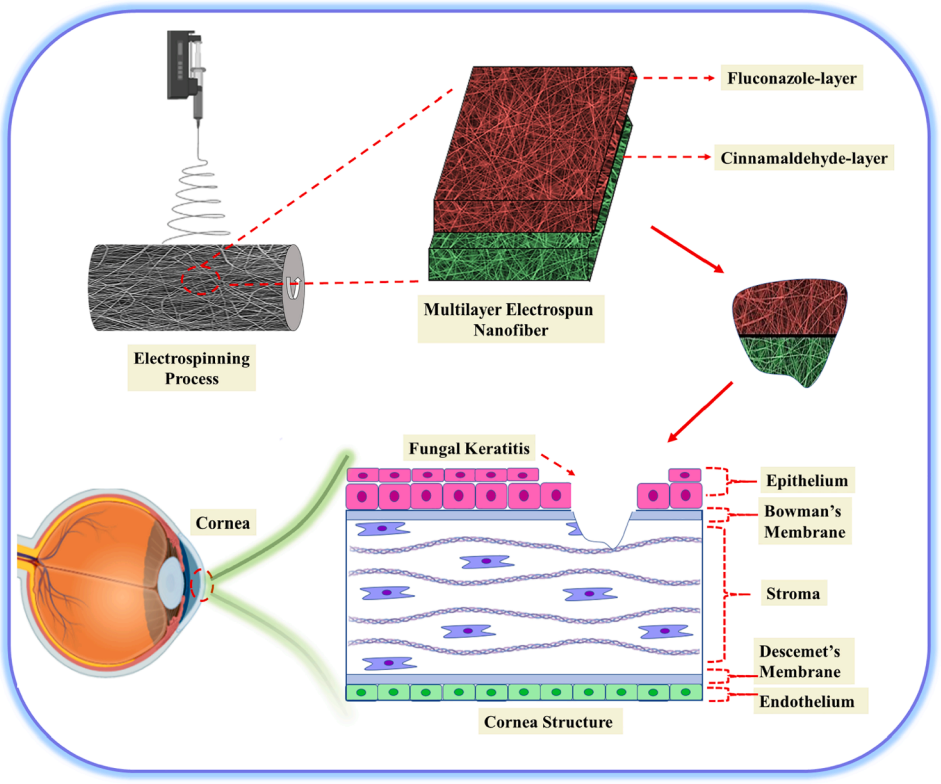

Fig. 1. Schematic presentation of the fabrication of multilayer electrospun nanofibers for corneal tissue engineering application.

electrospun nanofibers, scanning electron microscopy (SEM, EVO LS 10, Zeiss) was used. Prior observations, all electrospun nanofibers were coated with a gold−palladium layer by sputtering the samples for 120 s using the Quorum SC7620 Mini Sputter Coater. The average nanofiber diameter was calculated using imaging software (Olympus AnalySIS, USA).

2.6. Fourier transform infrared spectroscopy (FT-IR)

Fourier-transformed infrared spectroscopy (FTIR) analysis was performed with a Jasco FT/ IR-4700 model machine. All spectra were recorded in transmission mode over the 4000–400 cm^{-1} scan range, and 32 scans were averaged at 4 cm^{-1} resolution.

2.7. Differential scanning calorimetry (DSC)

Differential scanning calorimetry (DSC) (Shimadzu, Japan) was used to determine the thermal properties of the sample as glass transition temperature (Tg) and melting temperature (Tm). Temperature ranges were adjusted from 25 °C to 300 °C for all electrospun nanofiber groups. The adjusted heating rate for DSC measurements was 10°.

2.8. Mechanical properties

The mechanical properties of the electrospun nanofibers were analysed with a tensile testing machine (Shimadzu Corporation, EZ-LX, Kyoto, Japan). Before testing, the thickness of the nanofibrous meshes of different types was calculated using a digital micrometre (Mitutoyo MTI Corp., USA). The nanofibers had a dimension of 10 × 50 mm. For each group, three different samples were tested.

2.9. Swelling and degradation

The swelling and degradation properties of electrospun nanofibers were examined. The swelling test was applied using phosphate buffer saline (PBS) with a pH of 7.4. Electrospun nanofibers were immersed into 1 ml of buffer and placed in a thermal shaker (BIOSAN TS-100) at 37°. The initial weights of the nanofibrous meshes were recorded. The wet weights of the samples were measured daily. The swelling value (S) was calculated using Eq. (1) [22]:

$$D = \frac{W_w - W_O}{W_O}.100 \quad (1)$$

Fabricated electrospun nanofibers were placed in 1 ml PBS with pH 7.4 and held in the thermal shaker at 37° for the degradation test. At desired time points, samples were removed from PBS and dried in a drier at 37° for 24 h. The dried weights of the nanofibers were recorded. The degradation value (D) was calculated using Eq. (2) [23]:

$$D = \frac{W_0 - W_t}{W_O}.100 \quad (2)$$

2.10. Encapsulation efficiency, in vitro drug Release, and drug release kinetics

2.10.1. Encapsulation efficiency

The amount of drug-loaded in the nanofibers was calculated by performing the encapsulation efficiency (%EE) using a UV–VIS spectrophotometer (Shimadzu UV-3600, Kyoto, Japan). Initially, 5 mg of fibers was mixed until completely dissolved in solvent mixtures. A total of 1 ml was taken from each solution and investigated using a spectrophotometer All measurements were repeated three times for all three solutions. The %EE was calculated by the following equation [24];

$$EE\% = \frac{Themassofactualdrugloadedinnanofibers}{Massofdrugusedinnanofibersfabrication} \quad (3)$$

2.10.2. In vitro drug release

The in vitro release study of the drug-loaded nanofibers was performed in PBS at a pH of 7.4. 5 mg of drug-loaded electrospun nanofibers were immersed in 1 ml of PBS in a thermal shaker (BIOSAN TS-100, Riga, Latvia), constantly stirred and kept at 37 °C. At determined time intervals, 1 ml of release medium was removed and transferred to a UV spectrophotometer. The amount of the drug was measured. Every 1 ml was replaced with fresh PBS to continue the release studies.

2.10.3. Drug release kinetics

The zero-order, first-order, Korsmeyer–Peppas, Higuchi, and Hixson–Crowell models, which are different mathematical models, were used to evaluate and interpret the drug release kinetics from the nanofiber [25].

$$Q = Kt^n \quad (4)$$

$$Q = K_0 t \quad (5)$$

$$\ln(1 - Q) = -K_1 t \quad (6)$$

$$Q = K_h t_2^1 \quad (7)$$

$$Q_3^1 = K_{hc} t \quad (8)$$

In these equations, Q is the fractional amount of drug release at time t; K0, K1, K, Kh, and Khc are the kinetic constants for Zero-order, First-order, Korsmeyer-Peppas Higuchi, and Hixson-Crowell models, respectively. N is the diffusion exponent, which is indicative of the drug release mechanism.

2.11. In vitro antimicrobial activity

2.11.1. Antifungal activity test

The antifungal activities of GEL/PVA nanofibers containing CA and FLU were tested using the disc diffusion method described by the Clinical Laboratory Standards Institute (CLSI) (1). C. Albicans (ATCC 90023) strain was streaked on Sabouraud dextrose agar (SDA) and allowed to grow for 48 h at 37 °C. After 48 h, yeast suspension was prepared in physiological saline and adjusted to the turbidity of McFarland 0.5 cfu/ml. Then yeast suspension was spread onto Mueller-Hinton Agar +2% Glucose and 0.5 μg/mL Methylene Blue Dye Medium (GMB) using a sterile cotton swab. FLU and CA-loaded nanofibers cut into 6 mm discs were placed on the agar plates and incubated at 37 °C for 24 h. Inhibition zones were determined by measuring the zone diameters. FLU disc (25 μg) was used as a reference.

2.11.2. Biofilm formation assay

Biofilm formation in *C. albicans* ATCC 90023 was tested by modifying the crystal violet (CV) method described by Gulati et al. (2). *C. albicans strain* is grown on YEPD agar plate at 37 °C before biofilm assay. A single colony was inoculated into 4 ml YEPD broth and grown at 37 °C overnight. Then, cell density was adjusted to 1×10^7 cells/ml in RPMI 1640 medium. After that, the cells were incubated at 37 °C for 90 min by shaking at 140 rpm to allow the cells to attach. Unattached cells were removed by washing with 200 μL of PBS and fresh RPMI 1640 medium, and nanofiber discs (6 mm) containing FLU and CA were added and incubated at 37 °C for 24 h. The anti-biofilm efficiency of nanofibers was determined by staining biofilms with a 0.4% crystal violet solution. The biofilm-associated stain was measured at 595 nm by a microplate reader. Biofilm inhibition was calculated by:

$$BI\% = \frac{ODC - ODF}{ODC}.100 \quad (9)$$

%BI is the percentage of biofilm inhibition, ODC is the 595 nm absorbance value of control (without nanofibers), and ODF is the 595 nm absorbance value of the sample with nanofibers.

2.12. Cell culture test

2.12.1. Material sterilization

Material sterilisation was completed with UV light for 90 min under the Class II Laminar flow cabinet. After sterilisation, materials were placed onto the 96-well plate in favor of a 20 μL medium to ensure the stability of materials on the plate

2.12.2. Cell culture

GFP (green fluorescent protein) transfected human embryonic kidney (HEK) cell line was incubated in an incubator with 5% CO2 and 37 °C (Thermo) in the high glucose with 4.5 g/L D-Glucose, L-Glutamine, and sodium pyruvate Dulbecco's Modified Eagle Medium (DMEM) (NutriCulture, Ecobiotech) including 10% Fetal Bovine Serum (Gibco) and 1% penicillin–streptomycin (PAN Biotech). Cells were incubated in a humidified CO2 incubator. After cells reached 80% confluency on the flask, cells were detached using trypsin/EDTA (PAN Biotech), and collected cells were counted with Haemocytometer (Marienfield). Collected cells were centrifugated at 1500 rpm for 5 min, and the cell pellet was dissolved with an appropriate amount of DMEM to obtain 2,500 cells per 100 μL. In addition, 100 μL of cell solution was seeded onto each well for cell viability tests. The cell seeding was applied to 7-day, 3-day, and 1-day treatment materials.

2.12.3. Cell Viability- MTT assay

The MTT assay was achieved by using HEK cells with 2,500 cells/100 μL cell density. The cells were seeded on the materials to obtain 7-day, 3-day, and 1-day incubation time and understand cell-material interaction. The cellular proliferation and cellular viability results were calculated with the same MTT assay with different calculation techniques (for proliferation, the mean of photometric results' of each sample was divided into the first day's control, while for the cellular viability, the division was obtained with the daily control).

2.12.4. Fluorescence imaging

GFP transfected HEK cells were seeded on the materials and treated for 7-days, 3-days, and 1-day. Under the favor of GFP, cellular attachment on the nanofibrous meshes was confirmed, and the cellular viability was evaluated with MitoTracker (5 mg/mL). The fluorescence images were taken with the relevant excitation and emission wavelengths via the ZOE fluorescent cell imager (BIORAD).

2.12.5. Scanning electron microscopy imaging

After cellular experiments were completed, the cells were fixed onto the materials with a fixation solution (acetic acid: methanol with a ratio of 1:3). The existing medium was discarded for the fixation procedure, and nanofibrous meshes were washed with PBS twice, and a fixation solution was added to the samples. Next, samples were incubated with a fixation solution for 10 min at room temperature on the shaker. After incubation, the fixation solution was discarded, and the constructs were

washed with distilled water twice. Afterwards, the samples were ready for SEM imaging, and the imaging was performed with 10 kV with SEM (EVO LS 10, Zeiss).

2.13. Statistical analysis

The statistical analysis was determined by using a single factor ANOVA analysis program. Measurements of the pore size were made successfully by using SPSS 17.0 analysis program. Statistical significance was defined as $p < 0.05$. All quantitative results are presented as the mean ± STD.

3. Result&discussion

3.1. Scanning electron microscope (SEM)

The surface morphologies of the produced nanofibrous meshes were analysed using SEM. In addition, the diameters of the obtained nanofibers were calculated by taking an average of 100 random readings for each sample, and diameter distribution graphs were created. SEM images and fiber diameter histograms are demonstrated in Fig. 2. Highly uniform and smooth nanofibers were formed without any occurrence of bead defects for all the non-drug and drug-loaded electrospun nanofibers. The mean diameters of PVA/GEL, PVA/GEL/FLU, PVA/GEL/CA, and PVA/GEL/COM nanofibers were measured as 229 ± 26 nm, 263 ± 41 nm, 263 ± 73 nm, and 334 ± 56 nm respectively. It was observed that there was an increase in the diameter of the drug-loaded nanofibers compared to the pure nanofibers. In particular, a sharp increase in diameter was observed for the combined nanofibers loaded with both types of drugs. Research has shown that this situation is supported by the fact that the drug loaded with pure nanofibers causes an increase in their diameter [25,26]. Taepaiboon et al. observed a higher increase in the diameter of PVA nanofibers loaded with indomethacin compared to non-loaded PVA nanofibers. They suggested that this situation was caused by the increase in the viscosity of the PVA solution resulting from indomethacin addition [27]. Moreover, no drug crystals or other types of

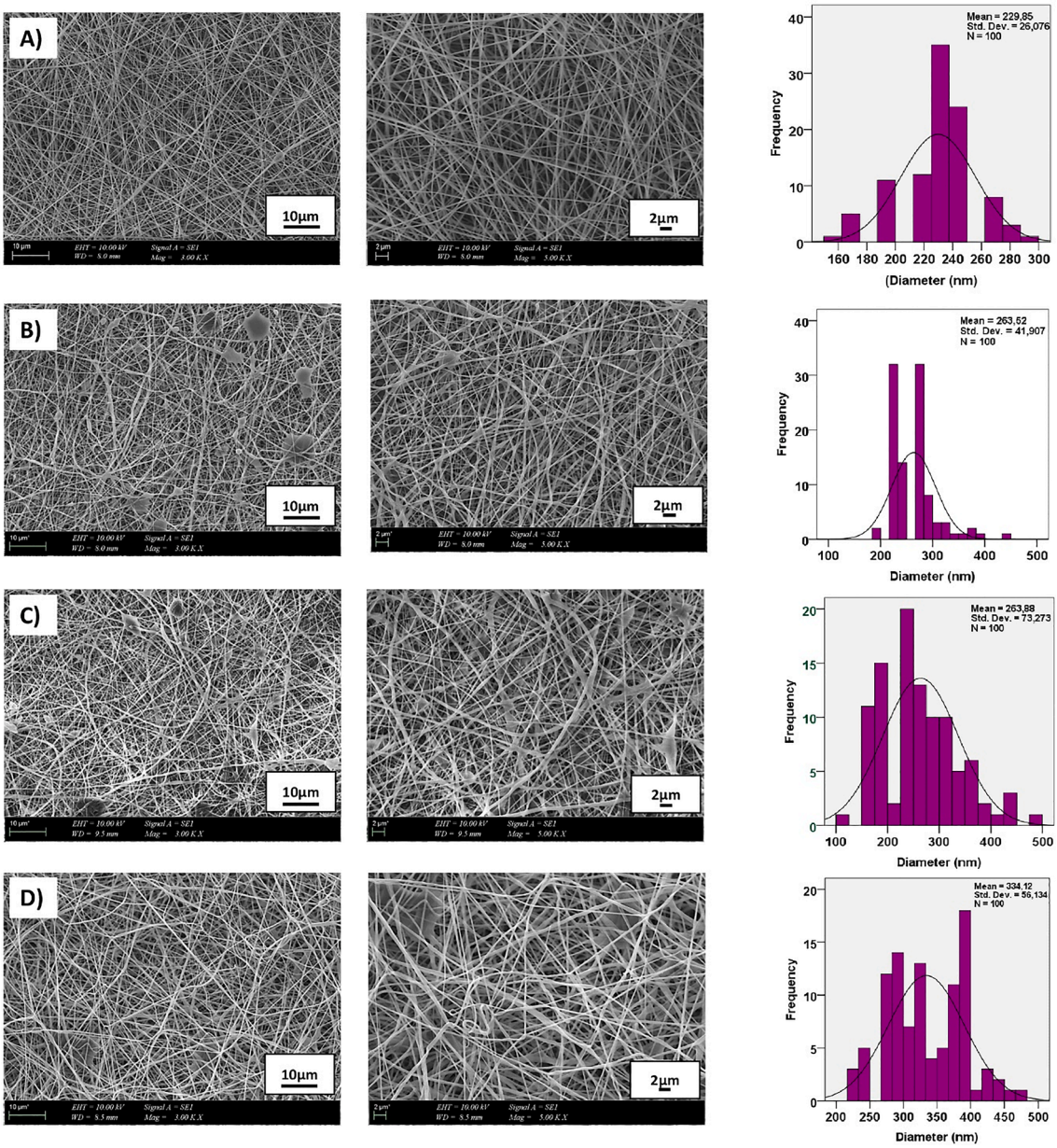

Fig. 2. Scanning electron microscopy images and fiber diameter distribution of nanofiber patches; PVA/GEL (a), PVA/GEL/FLU (b), PVA/GEL/CA (c), and PVA/GEL/COM (d).

drug aggregates appeared on the surface of either the PVA/GEL/CA or the PVA/GEL/COM nanofibers, especially despite the very low water solubility of CA. This is an important observation for both CA and all nanofibers, as it implies the excellent incorporation of the drugs into nanofibers [27].

3.2. Fourier transform infrared spectroscopy (FT-IR)

FTIR analysis was performed to examine the molecular structure and structural change of PVA/GEL/FLU and PVA/GEL/CA nanofibers. For pure GEL (Fig. 3A(a)), the appearance of absorption bands N—H stretching at 3277 cm^{-1}, C—H stretching at 2933 cm^{-1}, N—H bending at 1525 $cm^{-1,}$ and C—O stretching at 1626 cm^{-1} was observed [16]. For pure PVA (Fig. 3A(b)), sharp bands were seen at 3268 cm^{-1}corresponding to O—H stretching, at 2910 cm^{-1} C—H stretching of the alkyl groups, at 1646 cm^{-1} C═O and C—O stretching of the acetate groups, and at 1417 cm^{-1}C–H_2 stretching [16]. In Fig. 3A(c), the FTIR spectrum of CA shows a peak at 1670 cm^{-1},which belongs to C═O, due to the existence aldehyde group in its structure, and another peak at 1616 cm^{-1} belonging to the aromatic benzene ring in a merger with alkene [28,29]. In Fig. 3A(d), the appearance of a broad peak at 3200 cm^{-1} is due to the OH stretching, which confirms the presence of the hydroxyl group in FLU. The presence of a peak at 1620 cm^{-1}corresponds to C—N stretching indicating the presence of a triazole ring in FLU. Peaks at 1083 and 1112 cm^{-1} indicate the presence of two types of C—F bonds. Absorption bands in the region of 1504–1619 cm^{-1} indicate the C—C stretching of the aromatic ring, and 3060 cm^{-1} is due to the aromatic C—H stretching [30,31]. In Fig. 3B (e), the FTIR spectrum of the PVA/GEL had an almost equal spectrum with pure PVA besides the peak at 1261 cm^{-1}, which determined the peak of the pure PVA. It can be seen that the absorption band at 3270 cm^{-1} shifted to 3278 cm^{-1} with the GEL addition. Fig. 3B (f) is the absorbance spectrum of the PVA/GEL/CA. In the spectrum, CA addition affected the absorbance spectrum of the PVA/GEL at the same points with peak at 2906 cm^{-1}, 1419 $cm^{-1,}$ and 840 cm^{-1}. Fig. 3B (g), presents the specific vibrations at 2908 cm^{-1}, 1419 cm^{-1}, and 916 cm^{-1}caused by the FLU addition to the fibers. Characteristic peaks of all drugs were observed in PVA/GEL/COM fiber (Fig. 3B(h)). Thus, it is concluded that successful drug encapsulation was achieved.

3.3. Thermal behaviours of nanofibers

Chemical and physical changes such as phase transitions, glass transition temperature (Tg), and melting temperature (Tm) in the molecular structure of the material are determined by thermal characterisation techniques [32]. DSC thermograms of the electrospinning fibers of PVA/GEL, PVA/GEL/FLU, PVA/GEL/CA, and PVA/GEL/COM are represented in Fig. 4. PVA is a partially crystalline polymer exhibiting both the glass transition temperature, Tg (characteristic for amorphous phase), and melting isotherm, Tm (characteristic for crystalline phase) [33]. It was observed that the peaks observed in the DSC analysis belong to PVA, which has the highest content with all types of investigated nanofibers. The peak detected at 212.84 °C in the thermogram obtained for PVA/GEL represents the melting temperature of PVA. The peak at 59.42 °C can be associated with the relaxation of the amorphous region [16]. Moreover, the PVA/GEL nanofibers showed an endothermic curve with a peak of 190.98 °C. Glass transition temperatures for PVA/GEL/CA, PVA/GEL/FLU, and PVA/GEL/COM nanofibers were 61.07, 59.87, and 57.56 °C, respectively. It has been observed that the drugs added to the nanofibers resulted in small shifts to the glass transition temperature peak, which is not appreciable. One of the glass transition temperature's peak observed in all nanofibers may be due to the interactions between polymers [34]. Melting point temperatures of PVA/GEL/CA, PVA/GEL/FLU, and PVA/GEL/COM nanofibers were measured at 218.09, 219.24, 219.21 °C, respectively. It hypothesised that the amount of added drugs causes small shifts.

3.4. Mechanical properties of nanofibers

The mechanical property of ocular transplants is an important consideration for long-term durability and resistance to damage during use [21]. Interactions between the chemical structure of materials affect the tensile behaviour of nanofibers [35]. Both the tensile strength and strain at break of the produced electrospun nanofibrous meshes were investigated, and the results are shown in Fig. 5. The PVA/GEL electrospun nanofibrous meshes presented a tensile strength of 8.86 ± 0.42 MPa and a strain at a break of 26.9 ± 4.3. When drugs were loaded into these PVA/GEL electrospun nanofibers separately, and in combination, the tensile strengths were 7.96 ± 0.1, 8.5 ± 0.5, 7.19 ± 0.6 MPa, respectively. The strain at break is 18.32 ± 0.7, 19.25 ± 3.1, and 16.28

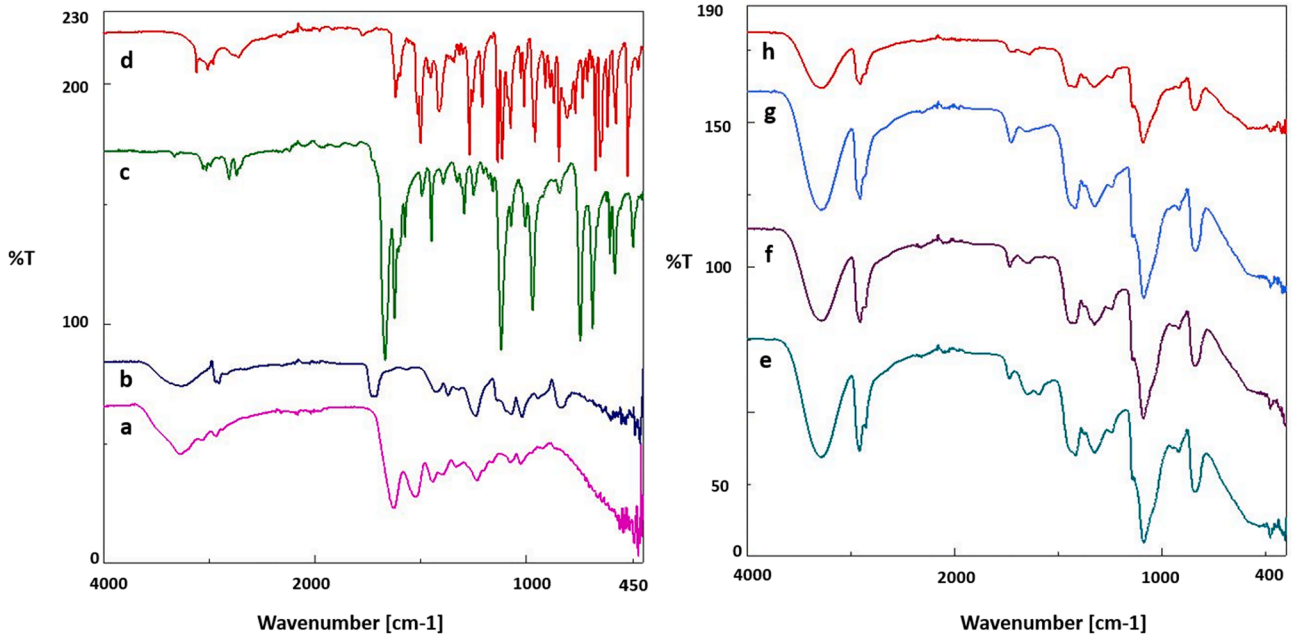

Fig. 3. FTIR spectra of (A) pure GEL (a), pure PVA (b), CA (c), FLU (d), (B) PVA/GEL (e), PVA/GEL/CA (f), PVA/GEL/FLU (g), PVA/GEL/COM (h) nanofibers.

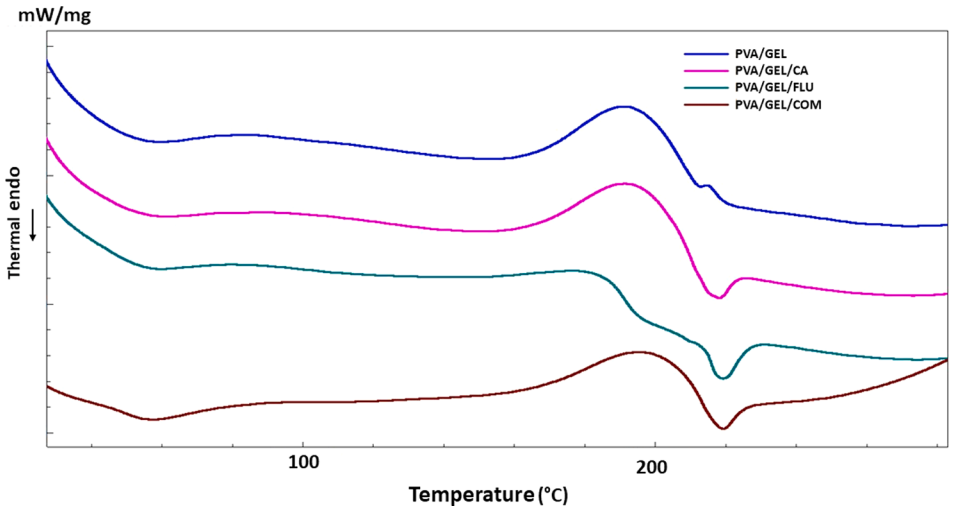

Fig. 4. DSC thermograms of the electrospun nanofibers.

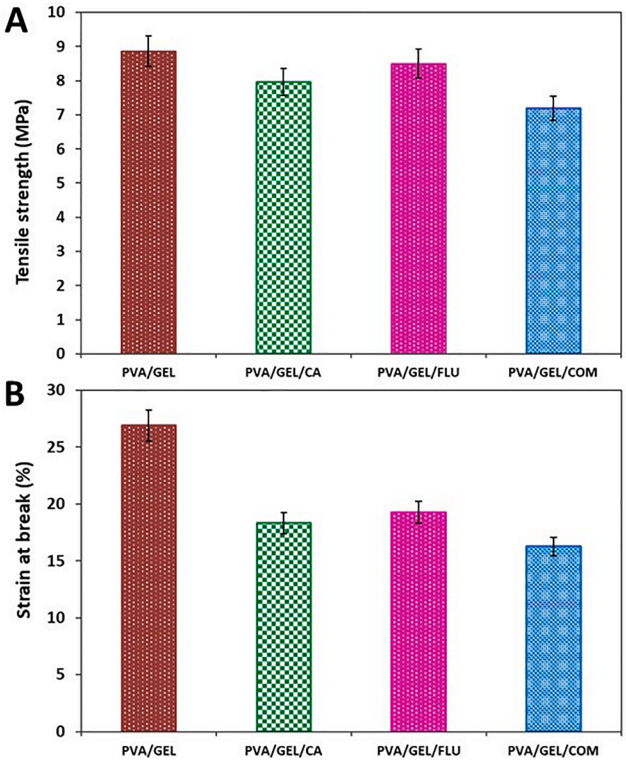

Fig. 5. Tensile test measurements of electrospun nanofibers: (a) tensile strength and (b) strain at break.

± 7.2 %, respectively. It seems that loading CA, and FLU drugs into the PVA/GEL electrospun nanofiber decreased its tensile strength. However, in the case of the combination of these drugs, the reduction was lower than for both single drug-loaded electrospun nanofibers. Cam et al. observed that when they loaded the drug into electrospun nanofibers, the mechanical properties decreased [25]. In addition, the effect of fiber diameter on mechanical properties can be explained by increases in fiber diameter and dispersion, as indicated in Fig. 4. As the drugs were loaded into the PVA/GEL electrospun nanofibers, increases in fiber diameter and dispersion were observed.

3.5. Swelling and degradation behaviours of nanofibers

The water absorption property of the nanofibrous structures produced for tissue engineering applications allows the transport of nutrients and oxygen [36]. Fig. 6 (a) represents the water uptake ratios of the nanofibers at 37 °C. According to Fig. 6, it can be observed that the drug-free pure nanofibers exhibit a swelling profile up to the 6th day and then begins to degrade. It can be observed that CA and FLU-loaded scaffolds have similar swelling rates compared to pure nanofiber, and the degradation accelerates by the 8th day. It can also be seen that PVA/

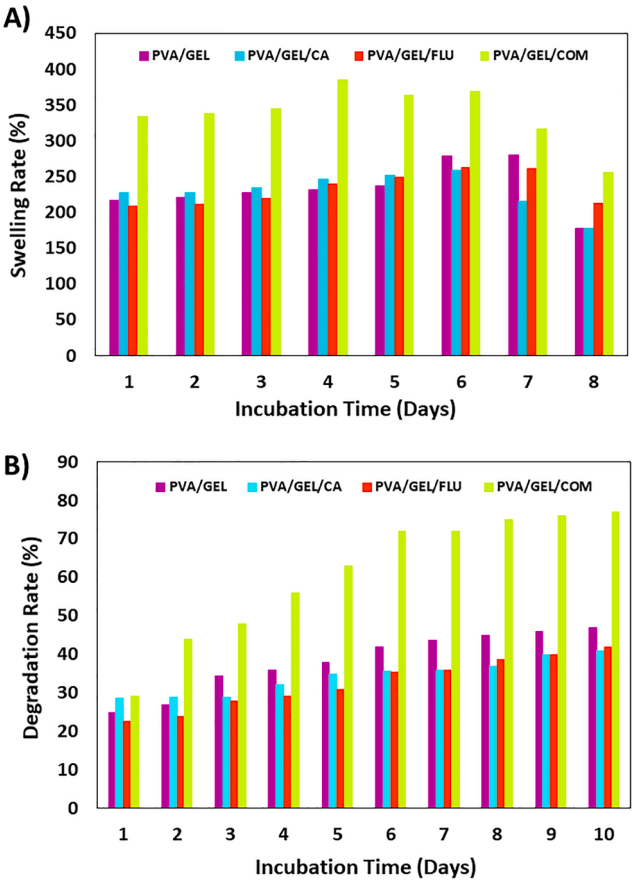

Fig. 6. Swelling (a) and Degradation (b) behaviours of electrospun nanofibers.

GEL/COM fiber shows higher swelling compared to other fibers by almost 400%. Cruz et al. research suggested that there is a correlation between the increase in the diameter of the fibers and the increase in the water absorption behaviour [37]. In this study, the highest swelling of PVA/GEL/COM fibers can be attributed to the thickest diameter of the fibers within its structure. Other groups of fibers showed the nearly same rate of swelling, as they reached a 250 % swelling rate on the 6th and 7th days.

Degradation is an essential factor for tissue engineering because biomaterials provide an environment for cell proliferation and implanted scaffolds should degrade after regeneration is completed [38]. In the degradation process, materials exposed to PBS dissolve and lose weight over time [39]. As shown in Fig. 6(b), the PVA/GEL/COM group exhibited a higher degradation rate compared to the other groups. Ilhan et al. reported that materials that have good water uptake capacity show good degradation properties [40]. All groups of the fibers exhibited a proportional degradation rate. When Ngawhirunpat et al. examined the degradation capacity of PVA nanofibers loaded with different concentrations of Meloxicam, they observed that the degradation behaviour of PVA nanofibers increased as the amount of drug they loaded increased [41].

3.6. Drug release kinetics

In this study, in vitro, drug release tests were performed to investigate the release properties of different drugs from three-layer electrospun nanofibers produced for fungal keratitis. First, the UV spectra obtained for all three drugs in the concentration range of 2 to 10 μg/mL CA, FLU and CA (R^2 = 0.8968), and FLU (R^2 = 0.9921) absorption values, and a linear standard calibration curve was plotted (Figs. 7 and 8). Released CA was detected at UV 280 nm absorbance, while FLU was detected at UV 260 nm absorbance. Apart from this, the encapsulation efficiency (EE) of all three drugs into nanofibers was determined. Encapsulation efficiency in CA and FLU-loaded nanofibers was determined as 73.84% and 68.58%, respectively (Figs. 7 and 8).

Drug release studies were performed in phosphate-buffered saline to mimic physiological conditions. When the CA release in the lowest layer is examined, it can be seen that it exhibits a controlled release profile that continues until the 96th hour (Fig. 7). It is observed that 87% of CA is released up to the first 8 h, exhibiting a burst release profile. The hydrophobic nature and high volatility of CA, which is only a small part of the hydroxyl group, is polar, and the solubility of CA in water is very low (1.35 g L^{-1}) [42]. This may be attributed to the release of most of the drug amount in a short period. Mishra et al. investigated drug release behaviour from CA-loaded gellan/PVA nanofibers in their study. It was found that the entire drug was released within 60 min, with an encapsulation efficiency of 17%, which is also attributed to a smaller amount of drug loadings and also to the hydrophobic nature of CA [13]. Compared to the above study, this research is expected to increase the amount of encapsulation and prolong drug release with higher drug loading. In addition, cross-linking nanofibers at 60 °C for 3 h with GA vapor is already expected to prolong drug release. The higher cross-linking caused the lower drug diffusion ratio out of the fiber matrix [43].

It can be observed that FLU, which shows a burst release by releasing 61% of the drug within the first 12 h, exhibits a release profile that extends up to 168 h(Fig. 8). It can be noticed that the hydrophilic nature and water solubility of FLU cause better integration within the PVA/GEL nanofibers and prolong the release with the effect of the cross-linking.

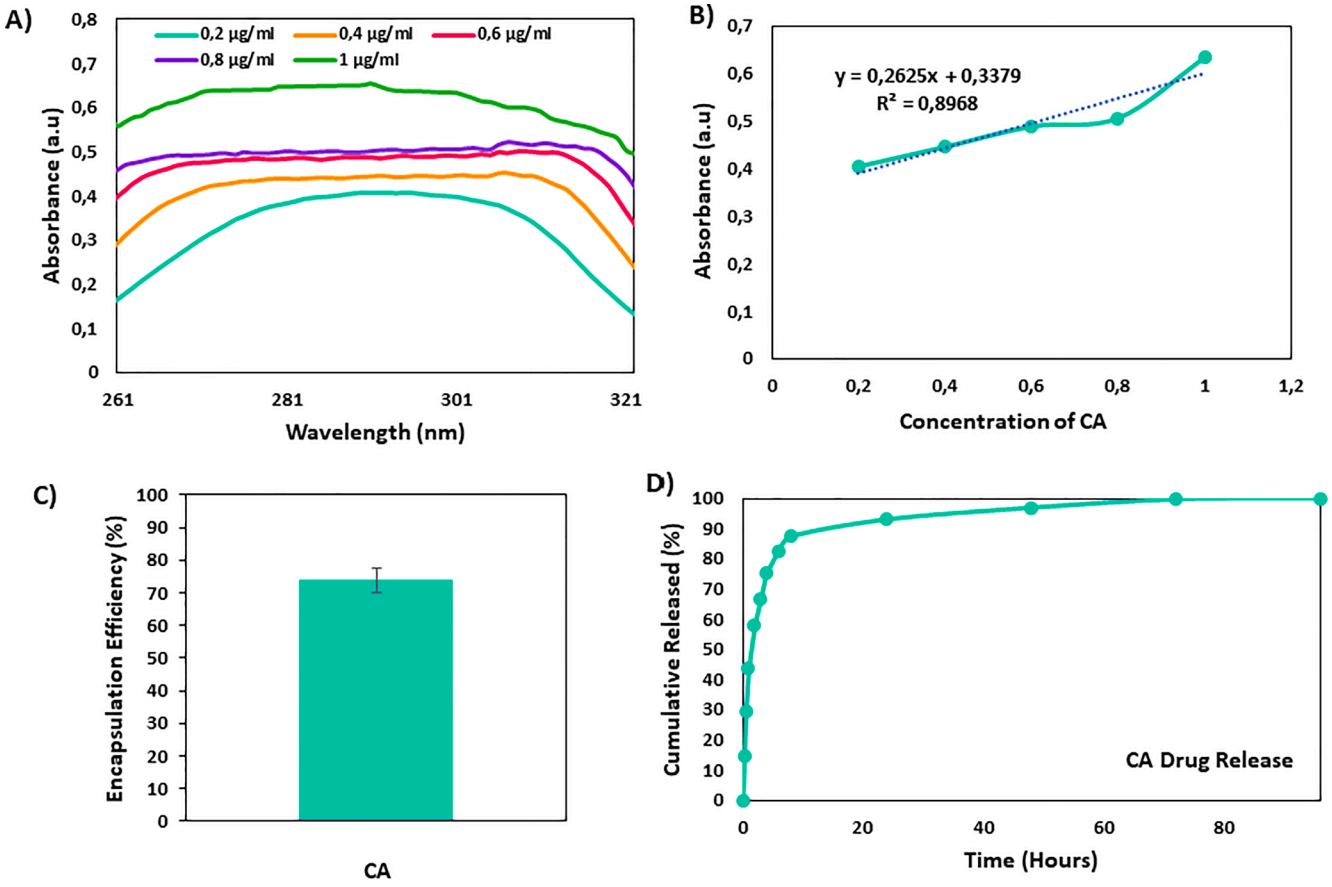

Fig. 7. In vitro drug release profiles of PVA/GEL/CA nanofiber: Absorption spectra of CA at different concentrations (a), CA calibration curve (b), encapsulation efficiency of PVA/GEL/CA nanofiber (c), drug release profiles from the PVA/GEL/CA electrospun nanofiber (d). All the measurements were repeated three times, and the errors were less than 5%.

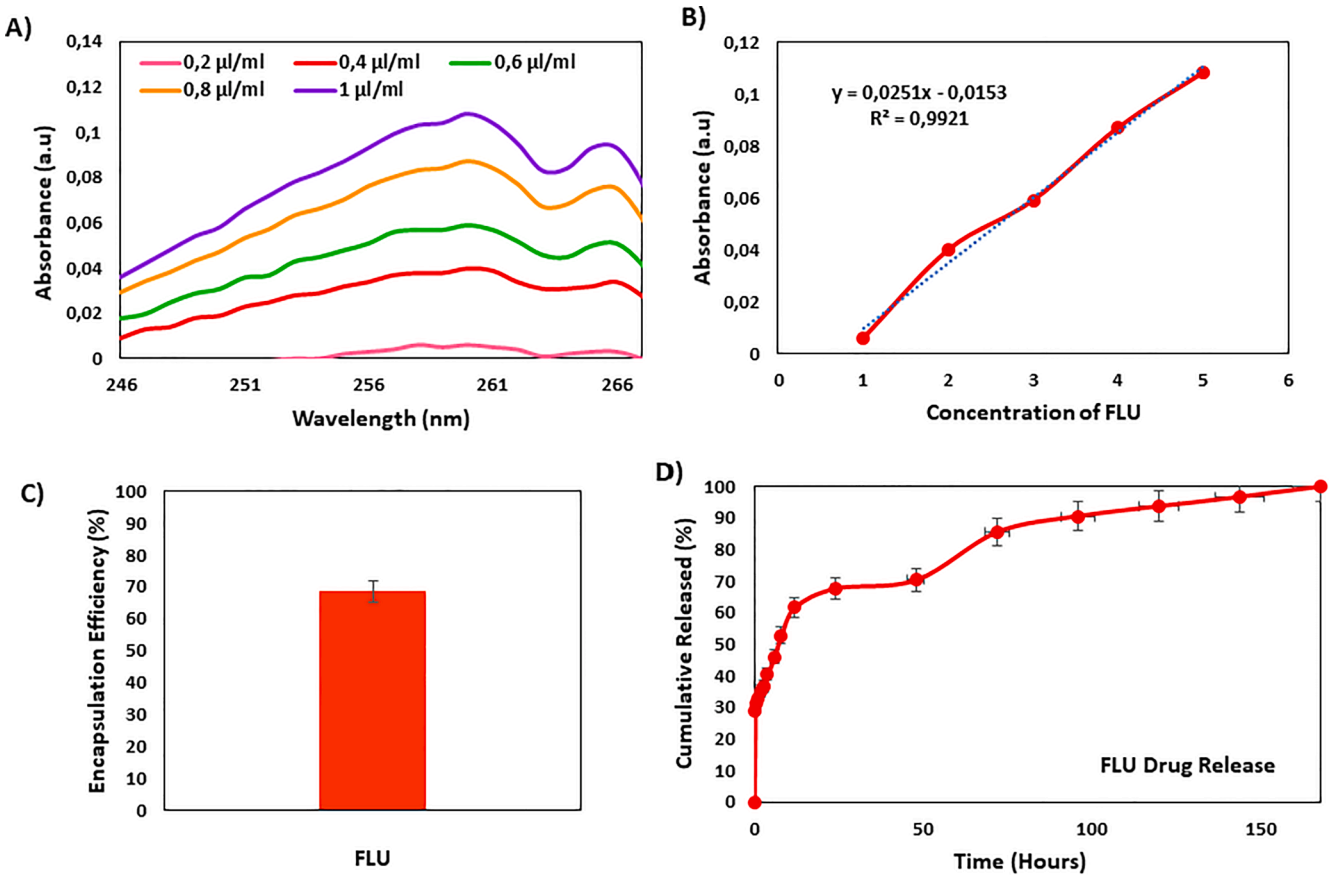

Fig. 8. In vitro drug release profiles of PVA/GEL/FLU nanofiber: Absorption spectra of FLU at different concentrations (a), FLU calibration curve (b), encapsulation efficiency of PVA/GEL/FLU nanofiber (c), drug release profiles from the PVA/GEL/FLU electrospun nanofiber (d). All the measurements were repeated three times, and the errors were less than 5%.

When PVA nanofibers are cross-linked with GA vapor, acetyl bridges are formed between the aldehyde ends of GA and the hydroxyl groups of the nanofibers, which reduces their water solubility. In this study, all nanofibers were cross-linked with GA vapor for 3 h, resulting in a more controlled release for all three drugs [43].

The release kinetics of PVA/GEL/CA and PVA/GEL/FLU nanofibers were investigated by Korsmeyer-Peppas, Zero-Order, First-Order, Higuchi, Hixon-Crowell models (Fig. 9). The kinetic constants and regression coefficients (R2) of all nanofibers are given in Table 2. In general, the most suitable mathematical model of the nanofiber with the highest correlation coefficient was evaluated. According to the highest regression coefficient obtained, it is seen that PVA/GEL/FLU nanofibers support the first-order model of drug release. In contrast, PVA/GEL/CA nanofibers support the Higuchi model (Fig. 9). Apart from this, n values corresponding to different transport mechanisms were correlated according to the Korsmeyer-Peppas model. The ranges of 'n' values illuminating the drug release mechanism from polymeric materials are as in Table 3 in the literature [44]. According to Table 3, the high value of ''n'' in the release mechanisms associated with the Korsmeyer-Peppas model indicates that it exhibits the Super-Case-II release mechanism. Super Case-II represents the release mechanism of hydrophilic polymer swelling in water or biological fluids as a result of chain relaxation [45].

3.7. Antifungal and antibiofilm activities of nanofibers

The antifungal activity of GEL/PVA nanofibers loaded with 0.2 % and 2.6 wt% FLU and CA respectively, was evaluated by the disc diffusion method. Twenty-five-microgram discs were prepared by pipetting 12.5-µl of stock FLU solution onto sterile blank discs as a reference. Inhibition zones were determined by measuring the zone diameters (Fig. 10). Disc diffusion test revealed that PVA/GEL/FLU and PVA/ GEL/COM nanofibers have antifungal activities against *Candida albicans*. The results of the antifungal activity of GEL/PVA nanofibers loaded with FLU and CA are shown in Table 4. As shown in Table 4, GEL/PVA/FLU/CA - mesh made of the combination of the nanofibers showed greater inhibitory activity (36 mm) than GEL/PVA/FLU alone nanofibers (28 mm). The addition of CA to PVA/GEL/FLU nanofibers enhanced the antifungal activity of fluconazole. Moreover, although PVA/GEL/COM nanofibers produced in this study contain less FLU (15 µg) than FLU discs (25 µg/disc) that is used for FLU susceptibility testing in routine clinical mycology laboratories, they exhibited better antifungal activity than 25 µg discs (Table 4).

The efficacy of FLU and CA-loaded PVA/GEL electrospun nanofibers in inhibiting *C. albicans* biofilm was also examined. It was observed that PVA/GEL/CA, PVA/GEL/FLU and PVA/ GEL/COM nanofibers inhibited biofilm development of *Candida albicans* by 22%, 37%, and 49%, respectively (Fig. 11). As observed in the disc diffusion test, incorporation of CA to PVA/ GEL/FLU nanofibers resulted in increased antibiofilm activity.

The antibacterial and antibiofilm activity of CA-loaded polymeric nanofibers produced by the electrospinning process has been reported previously [46,47]. In these studies, the antibacterial and antibiofilm activity of CA-loaded polymeric nanofibers were tested mostly in bacteria. Only one examined the antibiofilm effect of CA incorporated gellan/PVA electrospun nanofibers against *Candida* biofilm [48]. To our knowledge, there is no report on the antifungal and antibiofilm effect of GEL/PVA electrospun nanofibers containing both FLU and CA against *Candida albicans*.

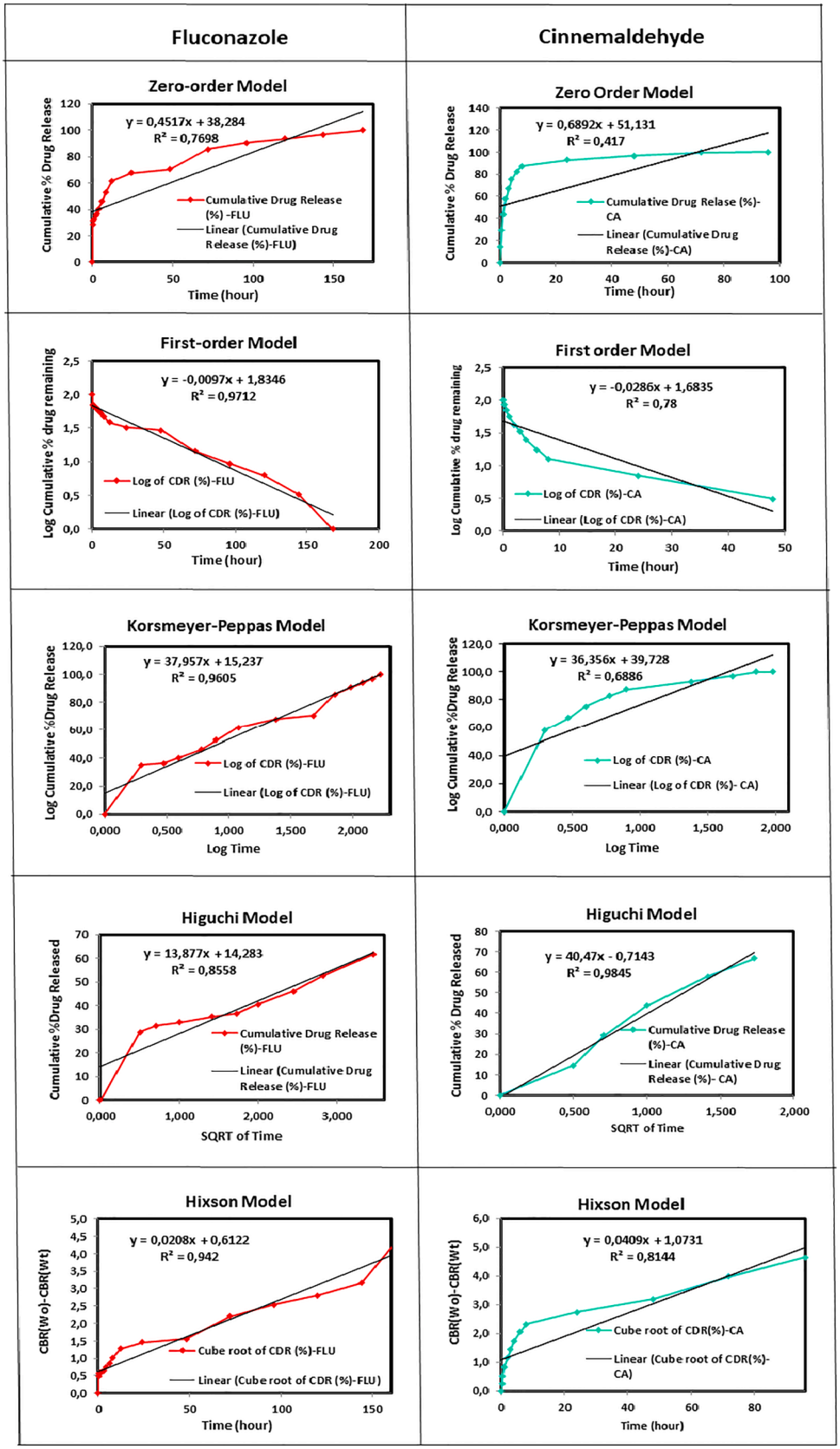

Fig. 9. Korsmeyer-Peppas, zero-order, first-order, Higuchi and Hixson-Crowell kinetic release patterns of FLU and CA drug release profiles.

Table 2
Transport mechanisms types according to the ranges of n value.

Sample	Korsmeyer-Peppas		Zero-Order		First-Order		Higuchi		Hixson-Crowell	
	R^2	n	R^2	K_0	R^2	K_1	R^2	K_h	R^2	K_{hc}
PVA/GEL/FLU	0.9905	37.957	0.7698	0.4517	0.9712	−0.0097	0.8558	13.877	0.942	0.0208
PVA/GEL/CA	0.6886	36.356	0.417	0.6892	0.78	−0.0286	0.9845	40.47	0.8144	0.0409

Table 3
Results of mathematical drug release models for all electrospun nanofibers.

The ranges of n values	Transport mechanisms
$0.45 \leq n$	Fickian diffusion mechanism
$0.45 < n < 0.89$	Non-Fickian transport
$n = 0.89$	Case II (relaxational) transport
$n > 0.89$	Super case II transport

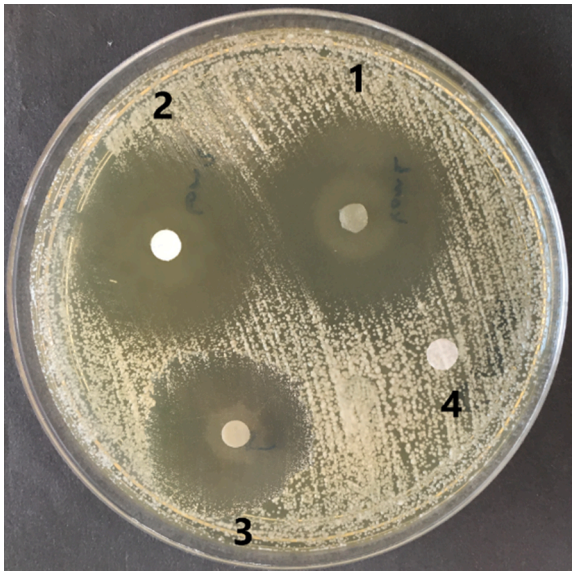

Fig. 10. Antifungal activities of PVA/GEL/FLU and PVA/GEL/COM nanofibers. 1. PVA/GEL/COM nanofiber, 2. FLU disc (control), 3. PVA/GEL/FLU nanofiber, and 4. PVA/GEL. All experiments were performed in triplicates, and data are presented as mean ± SD.

Table 4
Antifungal activity of PVA/GEL/CA and PVA/GEL/FLU nanofibers.

GEL/PVA Nanofibers	Diameter of zone of inhibition (in mm)
FLU (25 μg/disc)	35 ± 1
PVA/GEL/FLU (FLU(15 μg))	28 ± 1
PVA/GEL/COM (FLU(15 μg))	36 ± 1
PVA/GEL/CA	–

3.8. Cell culture assay

3.8.1. Cell viability

The cell viability and proliferation calculations were achieved by three technical replicates of one biological replicate because the error bar of the results was not shown on the graph (Fig. 12). The cell viabilities of nanofibers were similar to each other, and the cellular viabilities obtained for cells cultured in contact with all materials were higher than control nanofibers for 1-day and 3-day treatment; however, the cell viability decreased on the 7th-day of treatment (Fig. 12 (a)). This decrease could occur by reaching the confluency of cells for a seven-day incubation period and their detachment from the monolayer.

Cellular proliferation results obtained for the cells cultured on the electrospun nanofibers show that the proliferation was observed for 1-day and 3-day treatment, but the cellular amount decreased during the 7-day treatment (Fig. 12 (b)). The reduction in cell number was because of reaching confluency after 3-day treatment, and the cells started to detach.

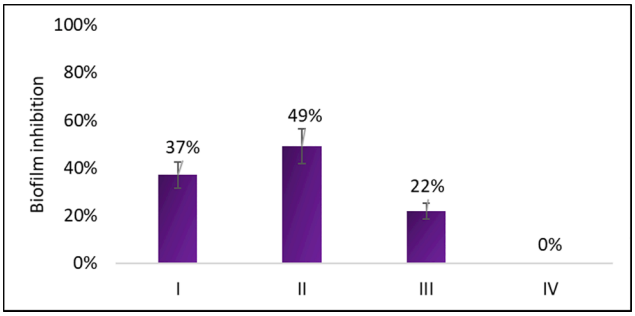

Fig. 11. Inhibition of *Candida albicans* biofilm by FLU and CA loaded nanofibers (I) PVA/GEL/FLU, (II) PVA/GEL/COM, (III) PVA/GEL/CA, (IV) PVA/GEL.

3.9. Fluorescence imaging

Fluorescence images were taken with MitoTracker staining methods, and the images in Fig. 13 represent the cells on the material. The fluorescence images were taken for 1-day and 3-day treatments (Fig. 13). The images showed that the cells found on the material surfaces as a cluster form, and the cellular proliferation could be observed over time. The scale of images was taken at 100 μm. Due to the materials' fluorescence luminance, the images were on a red background. Due to the property of MitoTracker dye, the viable cells had more fluorescence intensity. When comparing the feasible cells with controlled material (PVA/GEL), the PVA/GEL/FLU nanofiber had the highest attachment to the material with observed cellular morphology. The cells' clustering might be the cellular stress caused by foreign material; however, the cellular proliferation on the material was not affected. Fluorescence images of the materials showed that the materials have good biocompatibility.

3.10. SEM images

SEM images of samples were taken for 3-day treated, and 7-day treated electrospun nanofibers, and the scales of images were mainly 20 μm and 10 μm if not specified differently. For the PVA/GEL nanofiber, the SEM images showed that the diameter of the cells was smaller than the other materials; however, the cellular division and the attachment were observed on the 3-day and 7-day incubated materials. The cellular proliferation and migration were fewer than the other materials as well. For the PVA/GEL/FLU nanofiber, SEM images identified that the HEK cells were attached to the material, and they started to division on day three, and the cells were attached and spread (Fig. 14). The material PVA/GEL/CA was examined with SEM, and the cellular attachment was observed for both 3-day and 7-day attachment; however, the zoomed-in cell of the day three images indicated that the cells were attached to the material, but they started to become round-shape, and that means the cells were under stresses after a 3-day

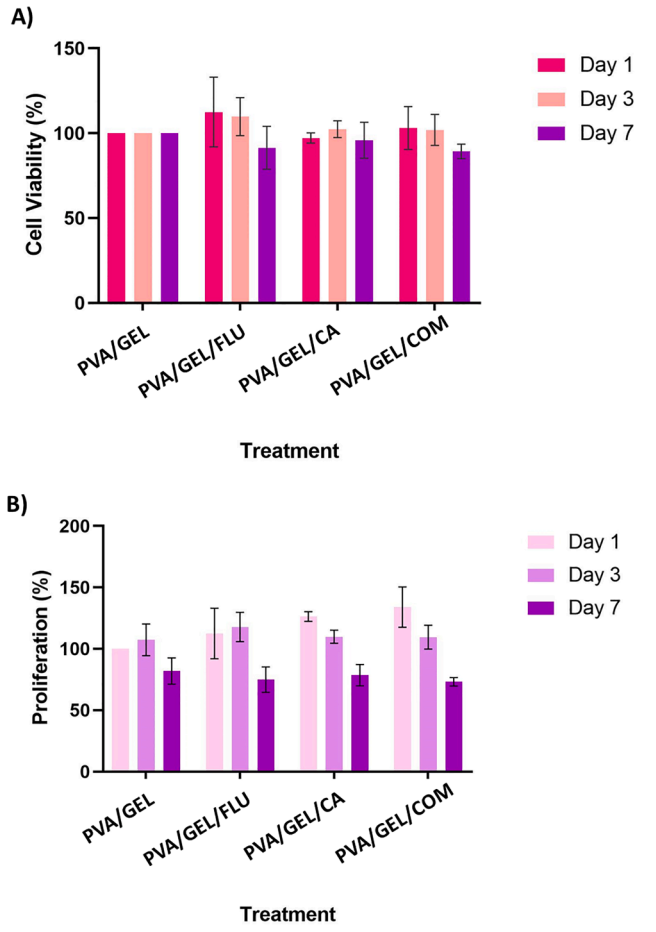

Fig. 12. (A) Cell viability results of 1-day, 3-day, and 7-day treated materials. PVA/GEL material was accepted as a control, and the calculations were compared with the controlled material. Results are the average value of three different technical replicates, which is estimated by relative cell viability ratio compared to Day 1 PVA/GEL treatment PVA/GEL, PVA/GEL/CA, PVA/GEL/FLU, PVA/GEL/COM. (B) The cellular proliferation rate of material-based treatment for three different treatment periods. Different colours represent day-based results. Results are the average value of three different technical replicates, which is estimated by relative cell viability ratio compared to Day 1 PVA/GEL treatment. PVA/GEL, PVA/GEL/CA, PVA/GEL/FLU, PVA/GEL/COM.

incubation with the material. Although the cellular stress was observed on the 3-day treatment, on the 7th day, the cellular attachment and proliferation were also observed with appropriate morphology. Therefore, the cellular attachment and cellular proliferation rate on the PVA/GEL/FLU nanofiber seemed better compared to other nanofibers. The nanofiber combination treatment for HEK cells for 3-day and 7-day SEM images was represented in Fig. 14. The cells were proliferated, and the cells spread around the nanofiber for both treatment periods; moreover, the cellular morphologies were stable during treatment.

The cellular experiments on the nanofibers showed that the materials' biocompatibility was applicable for HEK cells, and the materials promoted the proliferation and cellular attachment without any cytotoxic effect for a 7-day treatment period.

4. Conclusion

In this study, PVA/GEL, PVA/GEL/FLU, PVA/GEL/CA, and PVA/GEL/COM nanofibrous meshes, can be utilised to treat fungal keratitis were successfully produced. To increase the mechanical strength of the produced nanofibers and to prevent their rapid degradation, cross-linked with GA vapor was conducted. By loading the FLU and CA

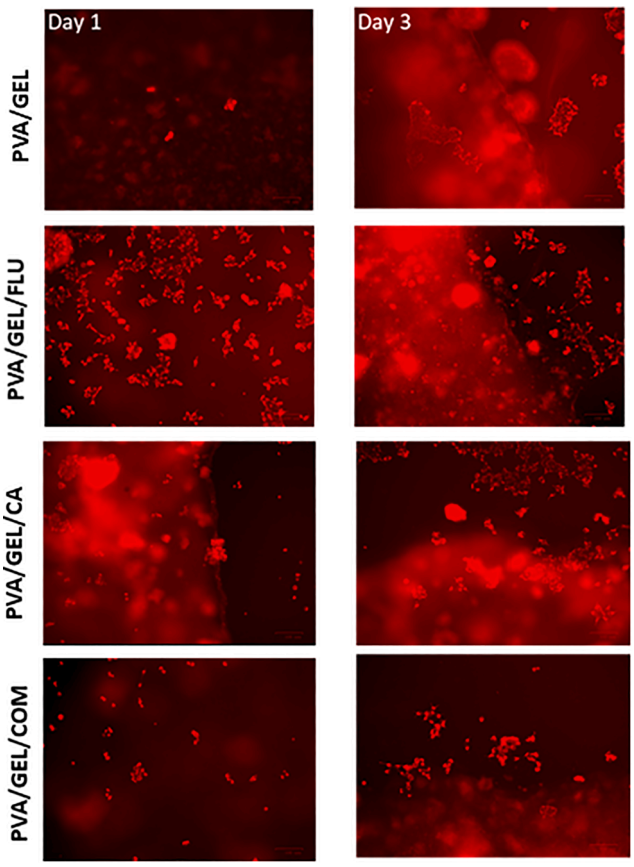

Fig. 13. Fluoresce images of viable cells on and the side of the material. The MitoTracker dye was used to obtain the images. The left side of the images belonged to a 1-day treatment, and the right side was of a 3-day treatment. The scale of images is 100 μm.

nanofiber layers separately, the yeast biofilm was blocked with CA present within the first layer. The yeasts were killed with FLU loaded within the second layer, thus increasing the drug efficacy and a treatment method was developed. According to the SEM results, although the increase in the amount of drug in the nanofiber caused a slight increase in the fiber diameters, it did not adversely affect the fiber morphologies. In particular, it can be noticed that the water absorption capacity of combination drug-loaded nanofibers is very high, and accordingly, they exhibit faster degradation. However, as the drug was applied, it was observed that the mechanical strength weakened compared to the pure nanofiber. Due to its hydrophobic nature, CA completed its release from nanofibers at 96 h, while FLU continued to release until 168 h. The fact that CA ends first and blocks the biofilm, and then the release of FLU continues supports the main logic of the research. In addition, both drugs showed a Korsmeyer-Peppas release kinetic profile with the highest R^2 value. In this study, FLU and CA-loaded electrospun nanofibers exhibited excellent efficacy against *C. albicans* growth and biofilm formation. The addition of CA into the PVA/GEL/FLU nanofibers increased the effect of FLU. Moreover, these nanofibers have no cytotoxic effect on human cells. Therefore, FLU and CA loaded PVA/GEL nanofibers can be successfully used in numerous medical applications such as corneal patches in the treatment of fungal keratitis.

CRediT authorship contribution statement

Elif Ilhan: Conceptualization, Methodology, Investigation, Writing – original draft. **Sumeyye Cesur:** Validation, Investigation, Writing – original draft. **Rabia Betul Sulutas:** Investigation, Writing – original draft. **Esra Pilavci:** Investigation, Writing – original draft. **Basak**

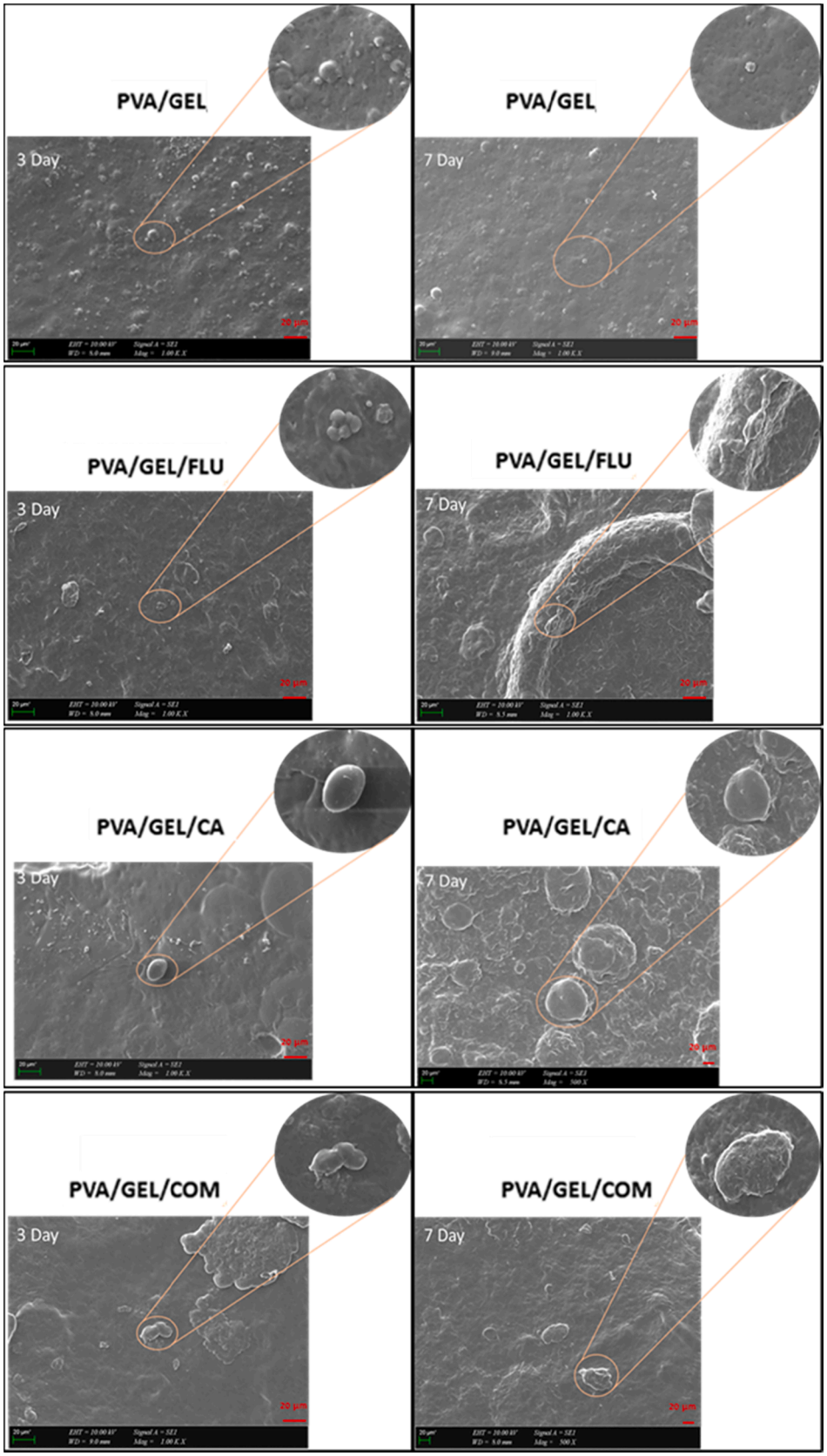

Fig. 14. SEM images of the materials of PVA/GEL, PVA/GEL/CA, PVA/GEL/FLU, PVA/GEL/COM, and com after 3-day treatment and 7-day treatment. The scale of the images was 20 μm, 30 μm, and 10 μm. The scale of the zoomed-in images was 10 μm.

Dalbayrak: Investigation, Writing – original draft. **Elif Kaya:** Investigation, Writing – original draft. **Elif Damla Arısan:** Writing – review & editing. **Gulgun Bosgelmez Tinaz:** Writing – review & editing. **Mustafa Sengor:** Writing – review & editing. **Ewa Kijeńska-Gawrońska:** Writing – review & editing. **Faik Nuzhet Oktar:** Writing – review & editing, Supervision, Project administration. **Oguzhan Gunduz:** Writing – review & editing, Supervision, Project administration.

Declaration of Competing Interest

The authors declare that they have no known competing financial interests or personal relationships that could have appeared to influence the work reported in this paper.

Data availability

Data will be made available on request.

Acknowledgements

This work was performed in the frame of the Marmara University Scientific Research Committee (Project Number: FDK-2021-10345) and the Polish-Turkish project - CorPatch - financially supported by TUBITAK (Project. No.120N333) and National Centre for Research and Development (Contract No. POLTUR4/CorPatch/1/2021). Elif Ilhan is a YÖK 100/2000 doctoral fellow in this research.

References

[1] Y. Acharya, B. Acharya, P. Karki, Fungal keratitis: study of increasing trend and common determinants, Nepal J. Epidemiol. 7 (2017) 685–693, https://doi.org/10.3126/NJE.V7I2.17975.
[2] Z. Ansari, D. Miller, A. Galor, Current thoughts in fungal keratitis: diagnosis and treatment, Curr. Fungal Infect. Rep. 7 (2013) 209–218, https://doi.org/10.1007/S12281-013-0150-110.1007/S12281-013-0150-1.
[3] Risk factors and clinical outcomes between fungal and bacterial keratitis: a comparative study – PubMed, (n.d.). https://pubmed.ncbi.nlm.nih.gov/9348453/ (accessed March 7, 2022).
[4] N. Sharma, J. Chacko, T. Velpandian, J.S. Titiyal, R. Sinha, G. Satpathy, R. Tandon, R.B. Vajpayee, Comparative evaluation of topical versus intrastromal voriconazole as an adjunct to natamycin in recalcitrant fungal keratitis, Ophthalmology. 120 (2013) 677–681, https://doi.org/10.1016/J.OPHTHA.2012.09.023.
[5] L. Brown, A.K. Leck, M. Gichangi, M.J. Burton, D.W. Denning, The global incidence and diagnosis of fungal keratitis, Lancet Infect. Dis. 21 (2021) e49–e57, https://doi.org/10.1016/S1473-3099(20)30448-5.
[6] I. Luis de Redín, C. Boiero, S. Recalde, M. Agüeros, D. Allemandi, J.M. Llabot, A. García-Layana, J.M. Irache, In vivo effect of bevacizumab-loaded albumin nanoparticles in the treatment of corneal neovascularization, Exp. Eye Res. 185 (2019) 107697, https://doi.org/https://doi.org/10.1016/j.exer.2019.107697.
[7] A. Urtti, Challenges and obstacles of ocular pharmacokinetics and drug delivery, Adv. Drug Deliv. Rev. 58 (2006) 1131–1135, https://doi.org/10.1016/j.addr.2006.07.027.
[8] J.F. Kernien, B.D. Snarr, D.C. Sheppard, J.E. Nett, The interface between fungal biofilms and innate immunity, Front. Immunol. 8 (2018) 1968, https://doi.org/10.3389/fimmu.2017.01968.
[9] X.Y. Sha, Q. Shi, L. Liu, J.X. Zhong, Update on the management of fungal keratitis, Int. Ophthalmol. 41 (2021) 3249–3256, https://doi.org/10.1007/S10792-021-01873-3.
[10] A. Panda, N. Sharma, S.K. Angra, Topical fluconazole therapy of Candida keratitis, Cornea. 15 (1996) 373–375, https://doi.org/10.1097/00003226-199607000-00007.
[11] S.N. Khan, S. Khan, J. Iqbal, R. Khan, A.U. Khan, Enhanced killing and antibiofilm activity of encapsulated cinnamaldehyde against candida albicans, Front. Microbiol. 8 (2017), https://doi.org/10.3389/fmicb.2017.01641.
[12] L. Chen, Z. Wang, L. Liu, S. Qu, Y. Mao, X. Peng, Y. Li, J. Tian, Cinnamaldehyde inhibits Candida albicans growth by causing apoptosis and its treatment on vulvovaginal candidiasis and oropharyngeal candidiasis, Appl. Microbiol. Biotechnol. 103 (2019) 9037–9055, https://doi.org/10.1007/s00253-019-10119-3.
[13] P. Mishra, P. Gupta, V. Pruthi, Cinnamaldehyde incorporated gellan/PVA electrospun nanofibers for eradicating Candida biofilm, Mater. Sci. Eng. C. 119 (2021) 111450, https://doi.org/https://doi.org/10.1016/j.msec.2020.111450.
[14] E. Kijeńska-Gawrońska, T. Bolek, M. Bil, W. Swieszkowski, Alignment and bioactive molecule enrichment of bio-composite scaffolds towards peripheral nerve tissue engineering, J. Mater. Chem. B. 7 (2019) 4509–4519, https://doi.org/10.1039/C9TB00367C.
[15] E. Kijeńska, W. Swieszkowski, 2 - General requirements of electrospun materials for tissue engineering: Setups and strategy for successful electrospinning in laboratory and industry, in: T. Uyar, E. Kny (Eds.), Electrospun Mater, Woodhead Publishing, Tissue Eng. Biomed. Appl., 2017, pp. 43–56, https://doi.org/https://doi.org/10.1016/B978-0-08-101022-8.00002-8.
[16] S. Ulag, E. Ilhan, R. Demirhan, A. Sahin, B.K. Yilmaz, B. Aksu, M. Sengor, D. Ficai, A.M. Titu, A. Ficai, O. Gunduz, Propolis-based nanofiber patches to repair corneal microbial keratitis, Molecules. 26 (2021) 2577, https://doi.org/10.3390/molecules26092577.
[17] M.E. Cam, A.N. Hazar-Yavuz, S. Cesur, O. Ozkan, H. Alenezi, H. Turkoglu Sasmazel, M. Sayip Eroglu, F. Brako, J. Ahmed, L. Kabasakal, G. Ren, O. Gunduz, M. Edirisinghe, A novel treatment strategy for preterm birth: Intra-vaginal progesterone-loaded fibrous patches, Int. J. Pharm. 588 (2020) 119782.
[18] F. Mohammadian, A. Eatemadi, Drug loading and delivery using nanofibers scaffolds, Artif. Cells, Nanomed. Biotechnol. 45 (2017) 881–888, https://doi.org/10.1080/21691401.2016.1185726.
[19] S. Ulag, E. Ilhan, B. Aksu, M. Sengor, N. Ekren, O. Kilic, O. Gunduz, Patch-Based Technology for Corneal Microbial Keratitis, in: Lect. Notes Comput. Sci. (Including Subser. Lect. Notes Artif. Intell. Lect. Notes Bioinformatics), 2020. <https://doi.org/10.1007/978-3-030-45385-5_18>.
[20] A. Arun, P. Malrautu, L. Anindita, S. Ramakrishna, Gelatin nanofibers in drug delivery systems and tissue engineering, Eng. Sci. 16 (2021) 71–81, https://doi.org/10.30919/es8d527.
[21] D. Jain, E. Carvalho, A.K. Banthia, R. Banerjee, Development of polyvinyl alcohol-gelatin membranes for antibiotic delivery in the eye, Drug Dev. Ind. Pharm. 37 (2) (2011) 167–177.
[22] E. Ilhan, Z. Karahaliloglu, E. Kilicay, B. Hazer, E.B. Denkbas, Potent bioactive bone cements impregnated with polystyrene-g-soybean oil-AgNPs for advanced bone tissue applications, Mater. Technol. 35 (3) (2020) 179–194.
[23] E. Ilhan, S. Ulag, A. Sahin, N. Ekren, O. Kilic, F.N. Oktar, O. Gunduz, Production of 3D-printed tympanic membrane scaffolds as a tissue engineering application, in: Lect. Notes Comput. Sci. (Including Subser. Lect. Notes Artif. Intell. Lect. Notes Bioinformatics), 2020. <https://doi.org/10.1007/978-3-030-45385-5_16>.
[24] M.E. Cam, S. Cesur, T. Taskin, G. Erdemir, D.S. Kuruca, Y.M. Sahin, L. Kabasakal, O. Gunduz, Fabrication, characterization and fibroblast proliferative activity of electrospun Achillea lycaonica-loaded nanofibrous mats, Eur. Polym. J. 120 (2019) 109239.
[25] M.E. Cam, B. Ertas, H. Alenezi, A.N. Hazar-Yavuz, S. Cesur, G.S. Ozcan, C. Ekentok, E. Guler, C. Katsakouli, Z. Demirbas, D. Akakin, M.S. Eroglu, L. Kabasakal, O. Gunduz, M. Edirisinghe, Accelerated diabetic wound healing by topical application of combination oral antidiabetic agents-loaded nanofibrous scaffolds: an in vitro and in vivo evaluation study, Mater. Sci. Eng. C. 119 (2021) 111586.
[26] D. Semnani, M. Afrashi, F. Alihosseini, P. Dehghan, M. Maherolnaghsh, Investigating the performance of drug delivery system of fluconazole made of nano–micro fibers coated on cotton/polyester fabric, J. Mater. Sci. Mater. Med. 28 (2017) 175, https://doi.org/10.1007/s10856-017-5957-9.
[27] P. Taepaiboon, U. Rungsardthong, P. Supaphol, Drug-loaded electrospun mats of poly(vinyl alcohol) fibres and their release characteristics of four model drugs, Nanotechnology. 17 (2006) 2317–2329, https://doi.org/10.1088/0957-4484/17/9/041.
[28] H. Chen, X. Hu, E. Chen, S. Wu, D.J. McClements, S. Liu, B. Li, Y. Li, Preparation, characterization, and properties of chitosan films with cinnamaldehyde nanoemulsions, Food Hydrocoll. 61 (2016) 662–671.
[29] B. Muhoza, S. Xia, J. Cai, X. Zhang, E. Duhoranimana, J. Su, Gelatin and pectin complex coacervates as carriers for cinnamaldehyde: effect of pectin esterification degree on coacervate formation, and enhanced thermal stability, Food Hydrocoll. 87 (2019) 712–722.
[30] N. Indora, D. Kaushik, Design, development and evaluation of ethosomal gel of fluconazole for topical fungal infection, Int. J. Eng. Sci. Invent. Res. Dev. I (2015).
[31] M. Ghosh, S. Mandal, A. Roy, S. Chakrabarty, G. Chakrabarti, S.K. Pradhan, Enhanced antifungal activity of fluconazole conjugated with Cu-Ag-ZnO nanocomposite, Mater. Sci. Eng. C. 106 (2020) 110160.
[32] T. Siddaiah, P. Ojha, N.O.G.V.R. Kumar, C. Ramu, Structural, optical and thermal characterizations of PVA/MAA:EA Polyblend films, Mater. Res. 21 (2018), https://doi.org/10.1590/1980-5373-MR-2017-0987.
[33] S.L. Agrawal, A. Awadhia, DSC and conductivity studies on PVA based proton conducting gel electrolytes, Bull. Mater. Sci. 27 (2004) 523–527, https://doi.org/10.1007/BF02707280.
[34] S. Cesur, S. Ulag, L. Ozak, A. Gumussoy, S. Arslan, B.K. Yilmaz, N. Ekren, M. Agirbasli, D.M. kalaskar, O. Gunduz, Production and characterization of elastomeric cardiac tissue-like patches for Myocardial Tissue Engineering, Polym. Test. 90 (2020) 106613.
[35] A. Ricci, K.J. Olejar, G.P. Parpinello, P.A. Kilmartin, A. Versari, Application of Fourier transform infrared (FTIR) spectroscopy in the characterization of tannins, Appl. Spectrosc. Rev. 50 (5) (2015) 407–442.
[36] M. Peter, N.S. Binulal, S. Soumya, S.V. Nair, T. Furuike, H. Tamura, R. Jayakumar, Nanocomposite scaffolds of bioactive glass ceramic nanoparticles disseminated chitosan matrix for tissue engineering applications, Carbohydr. Polym. 79 (2) (2010) 284–289.
[37] R.d.C.A.L. Cruz, L.G.M. Diniz, H.M. Lisboa, M.V.L. Fook, Effect of different carboxylic acids as solvent on chitosan fibers production by wet spinning, Rev. Mater. 21 (2) (2016) 525–531.
[38] J.P. Martins, M.P.A. Ferreira, N.Z. Ezazi, J.T. Hirvonen, H.A. Santos, G. Thrivikraman, C.M. França, A. Athirasala, A. Tahayeri, L.E. Bertassoni, Chapter 4–3D printing: prospects and challenges, in: V. Uskoković, D.P. Uskoković (Eds.),

Nanotechnologies Prev, Elsevier, Regen. Med., 2018, pp. 299–379, https://doi.org/https://doi.org/10.1016/B978-0-323-48063-5.00004-6.
[39] E. Ilhan, S. Cesur, E. Guler, F. Topal, D. Albayrak, M.M. Guncu, M.E. Cam, T. Taskin, H.T. Sasmazel, B. Aksu, F.N. Oktar, O. Gunduz, Development of Satureja cuneifolia-loaded sodium alginate/polyethylene glycol scaffolds produced by 3D-printing technology as a diabetic wound dressing material, Int. J. Biol. Macromol. 161 (2020) 1040–1054.
[40] E. Ilhan, S. Ulag, A. Sahin, B.K. Yilmaz, N. Ekren, O. Kilic, M. Sengor, D. M. Kalaskar, F.N. Oktar, O. Gunduz, Fabrication of tissue-engineered tympanic membrane patches using 3D-Printing technology, J. Mech. Behav. Biomed. Mater. 114 (2020) 104219, https://doi.org/10.1016/j.jmbbm.2020.104219.
[41] T. Ngawhirunpat, P. Opanasopit, T. Rojanarata, P. Akkaramongkolporn, U. Ruktanonchai, P. Supaphol, Development of meloxicam-loaded electrospun polyvinyl alcohol mats as a transdermal therapeutic agent, Pharm. Dev. Technol. 14 (2009) 73–82, https://doi.org/10.1080/10837450802409420.
[42] Z.I. Yildiz, M.E. Kilic, E. Durgun, T. Uyar, Molecular encapsulation of cinnamaldehyde within cyclodextrin inclusion complex electrospun nanofibers: fast-dissolution, enhanced water solubility, high temperature stability, and antibacterial activity of cinnamaldehyde, J. Agric. Food Chem. 67 (2019) 11066–11076, https://doi.org/10.1021/acs.jafc.9b02789.
[43] Z. Cui, Z. Zheng, L. Lin, J. Si, Q. Wang, X. Peng, W. Chen, Electrospinning and crosslinking of polyvinyl alcohol/chitosan composite nanofiber for transdermal drug delivery, Adv. Polym. Technol. 37 (2018) 1917–1928. <https://doi.org/https://doi.org/10.1002/adv.21850>.
[44] E. Saylam, Y. Akkaya, E. Ilhan, S. Cesur, E. Guler, A. Sahin, E. Cam, N. Ekren, F. Nuzhet Oktar, O. Gunduz, D. Ficai, A. Ficai, P. Calandra, D. Lombardo, Levodopa-Loaded 3D-Printed Poly (Lactic) Acid/Chitosan Neural Tissue Scaffold as a Promising Drug Delivery System for the Treatment of Parkinson&rsquos Disease, Appl. Sci. 11 (2021) 10727. <https://doi.org/10.3390/APP112210727>.
[45] D. Solanki, M. Motiwale, Studies on drug release kinetics and mechanism from sustained release matrix tablets of isoniazid using natural polymer obtained from dioscorea alata, Int. J. ChemTech Res. 13 (2020) 166–173, https://doi.org/10.20902/IJCTR.2019.130313.
[46] K.A. Rieger, J.D. Schiffman, Electrospinning an essential oil: Cinnamaldehyde enhances the antimicrobial efficacy of chitosan/poly(ethylene oxide) nanofibers, Carbohydr. Polym. 113 (2014) 561–568. <https://doi.org/https://doi.org/10.1016/j.carbpol.2014.06.075>.
[47] Y. Liu, X. Liang, R. Zhang, W. Lan, W. Qin, Fabrication of electrospun polylactic acid/cinnamaldehyde/β-cyclodextrin fibers as an antimicrobial wound dressing, Polymers (Basel) 9 (12) (2017) 464.
[48] P. Mishra, P. Gupta, V. Pruthi, Cinnamaldehyde incorporated gellan/PVA electrospun nanofibers for eradicating Candida biofilm, Mater. Sci. Eng. C. Mater. Biol. Appl. 119 (2021) 111450.